PHYSICAL REVIEW B VOLUME 61, NUMBER 18 1 MAY 2000-II

Localized folded acoustic phonon modes in coupled superlattices with structural defects

Ke-Qiu Chen and Xue-Hua Wang*
Institute of Physics, Academia Sinica, P.O. Box 603, Beijing 100080, China

Ben-Yuan Gu
CCAST (World Laboratory), P.O. Box 8730, Beijing 100080, China
and Institute of Physics, Academia Sinica, P.O. Box 603, Beijing 100080, China
(Received 20 September 1999; revised manuscript received 30 November 1999)

Using a transfer-matrix method, we investigate the property of the localized folded acoustic phonon modes in superlattices (SL's) with structural defect layers in the elastic approximation. We find that there exist localized folded acoustic phonon modes inside the minigaps of the coupled SL's grown along a cubic axis of bulk materials when introducing structural defect layers, and the frequency and the localization degree of these localized modes strongly depend on the widths of the structural cell and the defect layers. Moreover, we also notice an interesting change of the parity of the localized modes in the same minigap for different widths of defect layers.

I. INTRODUCTION

Since the proposal of semiconductor superlattices (SL's),[1] the fundamental properties of these structures have attracted a great deal of attention owing to their potential applications. The SL structures consist of periodically alternating thin layers of different materials, in which the thickness and material for each layer can be controlled with considerable accuracy due to a high level of perfection in the growth techniques of nanostructures. It is the great advance in microfabrication techniques that stimulates the experimental and theoretical studies on the physical properties of various SL structures.

The propagation of acoustic wave in the SL structures is one of the most important objects of physical investigation. It has received increasing interest due to the unusual physical properties observed in the SL structures in comparison with bulk materials. It has become a well-known fact that a periodic modulation of elastic stiffness constants in SL's changes the Brillouin zone to the zone-folded structures along the growth direction. As a result, the mini-Brillouin zone is formed and the folded phonon bands separated by minigaps appear. Theoretically, the properties of the folded acoustic phonon modes in various SL structures, such as infinite and semi-infinite SL's,[2–5] finite SL's,[6,7] and polytype SL's,[8,9] have been extensively investigated by using transfer-matrix and Green's-function methods. Experimentally, the Raman scattering,[10–14] the phonon transmission spectroscopy,[15] and the femtosecond time resolved pump-probe technique[16–20] are applied to explore the dispersion relations, minigaps, and coherence of the zone-folded phonon modes in the above-mentioned various SL structures.

Recently, one of extremely interesting subjects is to study the properties of localized modes in the coupled SL's, where an "artificial" defect layer is sandwiched by two semi-infinite SL's. It is well known that electronic structures of perfect SL's consist of a series of allowed minibands, i.e., continuum states are separated by the forbidden minigaps. Deviation of the structures from strict periodicity should result in the creation of bound states located within minigaps. This fact is well known from early studies of surface-terminated bulk crystal.[21] However, to our best knowledge, the previous experimental and theoretical studies on the coupled SL's with defect layers mainly focused on the properties of localized electrons and excitation states,[22–31] and the localization properties of phonon states in the coupled SL's were paid less attention.

The aim of this paper is to study the properties of the localized folded acoustic phonon modes lying within the opened minigaps in the phonon spectrum of the coupled SL's with defect layers. This paper is organized as follows: Sec. II gives a brief description of model and the necessary formulas used in calculations. The calculated results are presented in Sec. III with analyses. Finally, a summary is made in Sec. IV.

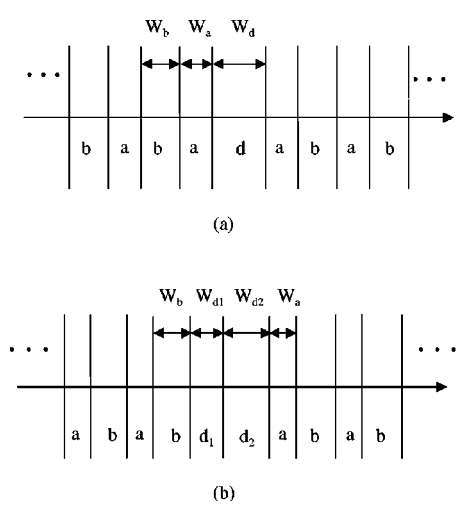

FIG. 1. (a) Schematic diagram of two semi-infinite SL's with an embedded structural defect layer *d*. W_d, W_a, and W_b, denote, respectively, the thickness of defect layer and constituent layers of the unit cell of the SL. (b) Schematic diagram of the SL with the binary structure defect layers. W_{d1} and W_{d2} are the thicknesses of the first and second defect layers, respectively. W_a and W_b are the thicknesses of the constituent layers of the unit cell of the SL.

II. MODEL AND FORMALISM

We consider two typical samples of the SL's with structural defects: (i) single structural defect SL, in which a defect layer is labeled as d (material AlAs) with a thickness of W_d embedded between two semi-finite superlattices with a cell unit composed of a (GaAs) and b (AlAs) materials, as shown in Fig. 1(a); (ii) binary structural defect SL, in which defect layers are labeled as $d1$ (GaAs) and $d2$ (AlAs) with the thickness of W_{d1} and W_{d2}, respectively, as shown in Fig. 1(b). In what follows, for simplicity, we chose Z axis parallel to the SL axis. For these structures, there exist pure longitudinal (L) and transverse (T) acoustic phonon modes, and transverse modes are twofold degenerate.

First, we investigate the localized L modes. For the localized phonon states, the Bloch wave number q_z should take a complex values in the form as

$$q_z=\frac{n\pi}{W}+iq \quad (q>0,\ n=1,2,3,\ldots), \tag{1}$$

where $W(=W_a+W_b)$ is the period of the SL's, $W_a(W_b)$ is the width of a (b) layer. The localized state solution of the elastic wave motion equation for L modes can be written as

$$\Phi(z,t)=U_L(z)e^{-i\omega t}, \tag{2}$$

where $U_L(z)$ represents the atomic displacement for localized L modes, and ω is the frequency of the localized modes. For the coupled SL's with structural defect layers, the corresponding atomic displacement in different layers can be expressed as

$$U_L(z)=\begin{cases} F(A^r_{Lj},B^r_{Lj},k_{Lj},z-z^r_{mj})e^{iq_z(m-1)W} & (-W_j/2\leqslant z-z^r_{mj}\leqslant W_j/2),\\ F(A_{Ld},B_{Ld},k_{Ld},z-z_d) & (-W_d/2\leqslant z-z_d\leqslant W_d/2),\\ F(A^l_{Lj},B^l_{Lj},k_{Lj},z-z^l_{mj})e^{iq_z(m-1)W} & (-W_j/2\leqslant z-z^l_{mj}\leqslant W_j/2),\end{cases} \tag{3}$$

where the function $F(A,B,k,z)$ is defined by

$$F(A,B,k,z)=Ae^{ikz}+Be^{-ikz}, \tag{4}$$

z_d is the center coordinate of the defect layer, z^l_{mj} and z^r_{mj} are the center coordinates of the jth$(j=a,b)$ layer in the mth $(m=1,2,3,\ldots)$ period of the left and right semi-infinite SL's; $k_{L\mu}$ is given by

$$k_{L\mu}=\frac{\omega_L}{\sqrt{\dfrac{C_{11,\mu}}{\rho_\mu}}} \quad (\mu=a,b,d). \tag{5}$$

$C_{11,\mu}$ is elastic stiffness constant in the μ layer, and ρ is the mass density.

By imposing boundary conditions at interfaces: the atomic displacement $U_L(z)$ and the force $C_{11}U'_L(z)$ should be continuous at each interface, we then obtain

$$\begin{pmatrix} A^l_{Lj}\\ B^l_{Lj}\end{pmatrix}=\hat{Q}\begin{pmatrix} A^r_{Lj'}\\ B^r_{Lj'}\end{pmatrix}, \tag{6}$$

$$\hat{S}^\beta\begin{pmatrix} A^\beta_{La}\\ B^\beta_{La}\end{pmatrix}=0 \quad (\beta=l,r), \tag{7}$$

where

$$\hat{S}^\beta=\begin{cases}\hat{I}-\hat{P}e^{iq_zW} & (\beta=r),\\ \hat{I}-\hat{P}e^{-iq_zW} & (\beta=l),\end{cases} \tag{8}$$

$$\hat{Q}=\hat{T}^{-1}(C_{11,j},k_{Lj},W_j)\prod_{i=1}^{s}\hat{M}(C_{11,di},k_{Ldi},W_{di})\times\hat{T}(C_{11,j'},k_{Lj'},-W_{j'}), \tag{9}$$

$$\hat{P}=\hat{T}^{-1}(C_{11,a},k_{La},W_a)\hat{M}(C_{11,b},k_{Lb},W_b)\times\hat{T}(C_{11,a},k_{La},-W_a), \tag{10}$$

with

$$\hat{M}(C,k,z)=\hat{T}(C,k,-z)\hat{T}^{-1}(C,k,z), \tag{11}$$

$$\hat{T}(C,k,z)=\begin{pmatrix} e^{ikz/2} & e^{-ikz/2}\\ iCke^{ikz/2} & -iCke^{-ikz/2}\end{pmatrix}. \tag{12}$$

Combining Eqs. (1), and (6)–(8), we derive the equations for determining the frequency ω and the decay factor q of the localized modes for longitudinal acoustic phonons as follows:

$$\cosh(qW)=0.5(-1)^n(\hat{P}_{11}+\hat{P}_{22}), \tag{13}$$

$$(-1)^n\sinh(qW)(\hat{Q}_{11}+\hat{Q}_{22})+0.5(\hat{P}_{22}-\hat{P}_{11})(\hat{Q}_{22}-\hat{Q}_{11})+\hat{P}_{12}\hat{Q}_{21}+\hat{P}_{21}\hat{Q}_{12}=0. \tag{14}$$

When $s=1$ and $j=j'=a$, the formulas above actually are for a single structural defect situation as shown in Fig. 1(a), while $s=2$, $j=b$, and $j'=a$, they become the ones for a binary structural defect situation as shown in Fig. 1(b).

Without losing generality, we now study the wave function of localized modes in SL's with binary structural defect layer corresponding to Fig. 1(b). In fact, as $W_{d1}=W_a$ or $W_{d2}=W_b$, the binary structural defect SL is reduced to a single structural defect SL. We introduce the relative coordinate in each layer as follows:

$$\tilde{Z}_{d1}=z-z_{d1} \quad (-W_{d1}/2\leqslant\tilde{Z}_{d1}\leqslant W_{d1}/2), \tag{15}$$

$$\tilde{Z}_{d2}=z-z_{d2} \quad (-W_{d2}/2\leqslant\tilde{Z}_{d2}\leqslant W_{d2}/2), \tag{16}$$

$$\tilde{Z}_a^m=z-z_a^m \quad (-W_a/2\leqslant\tilde{Z}_a^m\leqslant W_a/2), \tag{17}$$

$$\tilde{Z}_b^m=z-z_b^m \quad (-W_b/2\leqslant\tilde{Z}_b\leqslant W_b/2). \tag{18}$$

According to Eqs. (1), (3), and (4), the wave function of localized states can be expressed as

$$U_L(z)=\begin{cases} A_{La}^rF(A_{L\nu},B_{L\nu},k_{L\nu},\tilde{Z}_\nu)(\nu=d1,d2), \\ A_{La}^rF[1,(e^{-iq_zW}-\hat{P}_{11})/\hat{P}_{12},k_{La},\tilde{Z}_a]e^{iq_z(m-1)W}, \\ A_{La}^rF(A_{Lb}^r,B_{Lb}^r,k_{Lb},\tilde{Z}_b)e^{iq_z(m-1)W}, \\ A_{La}^rF(A_{L\zeta}^l,B_{L\zeta}^l,k_{L\zeta},\tilde{Z}_\zeta)e^{iq_z(m-1)W} \quad (\zeta=a,b), \end{cases} \tag{19}$$

where A_{La}^r is the normalized constant; q_z is determined by Eq. (13). By using boundary conditions at interfaces, we obtain

$$\begin{pmatrix} A_{Lb}^r \\ B_{Lb}^r \end{pmatrix}=\hat{S}_1\hat{A}, \tag{20}$$

$$\begin{pmatrix} A_{Ld2} \\ B_{Ld2} \end{pmatrix}=\hat{S}_2\hat{A}, \tag{21}$$

$$\begin{pmatrix} A_{Ld1} \\ B_{Ld1} \end{pmatrix}=\hat{S}_3\hat{A}, \tag{22}$$

$$\begin{pmatrix} A_{Lb}^l \\ B_{Lb}^l \end{pmatrix}=\hat{S}_4\hat{A}, \tag{23}$$

$$\begin{pmatrix} A_{La}^l \\ B_{La}^l \end{pmatrix}=\hat{S}_5\hat{A}, \tag{24}$$

with

$$\hat{A}=\begin{pmatrix} 1 \\ (e^{-iq_zW}-\hat{P}_{11})/\hat{P}_{12} \end{pmatrix}, \tag{25}$$

$$\hat{S}_1=\hat{T}^{-1}(C_{11,b},k_{Lb},-W_b)\hat{T}(C_{11,a},k_{La},W_a), \tag{26}$$

$$\hat{S}_2=\hat{T}^{-1}(C_{11,d2},k_{Ld2},W_{d2})\hat{T}(C_{11,a},k_{La},-W_a), \tag{27}$$

$$\hat{S}_3=\hat{T}^{-1}(C_{11,d1},k_{Ld1},W_{d1})\hat{T}(C_{11,d2},k_{Ld2},-W_{d2})\hat{S}_2, \tag{28}$$

$$\hat{S}_4=\hat{T}^{-1}(C_{11,b},k_{Lb},W_b)\hat{T}(C_{11,d1},k_{Ld1},-W_{d1})\hat{S}_3, \tag{29}$$

$$\hat{S}_5=\hat{T}^{-1}(C_{11,a},k_{La},W_a)\hat{T}(C_{11,b},k_{Lb},-W_b)\hat{S}_4. \tag{30}$$

In terms of the normalized condition of localized state wave functions: $\int_{-\infty}^{\infty}|U_L(z)|^2dz=1$, we have

$$A_{La}^r=\frac{1}{\sqrt{I_\nu+I_j^l+I_j^r}}, \tag{31}$$

with

$$I_\nu=\int_{-W_{d1}/2}^{W_{d1}/2}|F(A_{Ld1},B_{Ld1},k_{Ld1},\tilde{Z})|^2d\tilde{Z} + \int_{-W_{d2}/2}^{W_{d2}/2}|F(A_{Ld2},B_{Ld2},k_{Ld2},\tilde{Z})|^2d\tilde{Z}, \tag{32}$$

$$I_j^r=\frac{1}{1-e^{-2q_zW}}\left[\int_{-W_a/2}^{W_a/2}|F[1,(e^{-iq_zW}-\hat{P}_{11})/\hat{P}_{12},k_{La},\tilde{Z}]|^2d\tilde{Z} + \int_{-W_b/2}^{W_b/2}|F(A_{Lb}^r,B_{Lb}^r,k_{Lb},\tilde{Z})|^2d\tilde{Z}\right], \tag{33}$$

and

$$I_j^l=\frac{1}{1-e^{-2q_zW}}\left[\int_{-W_a/2}^{W_a/2}|F(A_{La}^l,B_{La}^l,k_{La},\tilde{Z})|^2d\tilde{Z} + \int_{-W_b/2}^{W_b/2}|F(A_{Lb}^l,B_{Lb}^l,k_{Lb},\tilde{Z})|^2d\tilde{Z}\right]. \tag{34}$$

Then we can easily write the wave functions of the localized modes in all layers according to the formulas above. All the above-mentioned formulas are also valid for the localized modes of the transverse acoustic phonons as long as $C_{11,\mu}$ is replaced by $C_{44,\mu}$.

In the following calculations, we employ the values of elastic stiffness constants and the mass densities presented in Ref. 32: $C_{11}=12.21(10^{10}\ \mathrm{Nm}^{-2}),C_{44}=5.99(10^{10}\ \mathrm{Nm}^{-2})$, and $\rho=5317.6(\mathrm{kgm}^{-3})$ for GaAs; $C_{11}=12.02$ $(10^{10}\ \mathrm{Nm}^{-2}),C_{44}=5.89(10^{10}\ \mathrm{Nm}^{-2})$, and $\rho=3760$ (kgm^{-3}) for AlAs.

III. NUMERICAL RESULTS AND ANALYSES

We first describe the influence of a-layer width W_a on the localized modes of longitudinal acoustic phonons. The calculated results are depicted in Fig. 2. We chose $W_b=8$ nm, $W_d=4$ nm, and the material of the defect layer d being the same as b (AlAs) material in calculations. The regions between two dotted lines in Figs. 2(a) and (c) represent the first and second minigaps and solid lines display the variation of frequency of two localized modes located in the first and second minigaps, respectively. Figures 2(b) and (d) show the dependence of the decay factor q of the localized modes on W_a, corresponding to the first and second localized modes, respectively.

From Figs. 2(a) and (c), it is clearly seen that minigaps always shift towards low frequency region as W_a increases. At the same time, the frequencies of localized modes are also

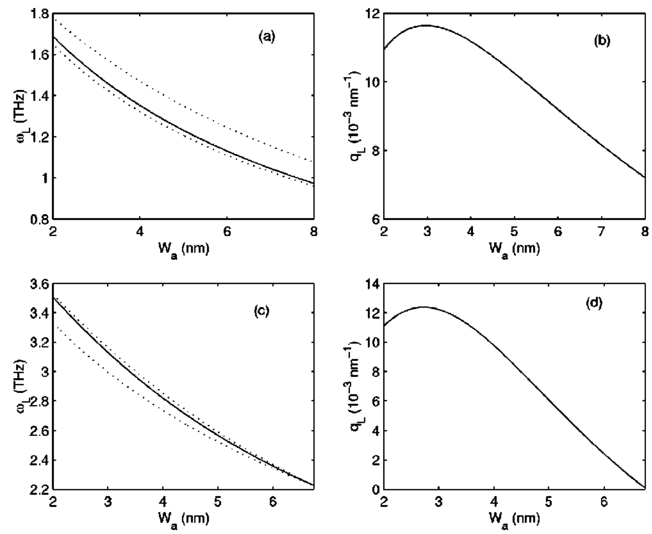

FIG. 2. Dependence of frequency ω and decay factor q of the localized L acoustic modes on the width W_a of the layer a in the coupled SL's with $W_b = 8$ nm and $W_d = 4$ nm. (a) and (b) correspond to the localized modes lying within the first minigap, (c) and (d) to the localized modes lying within the second minigap. The regions between two dotted lines in (a) and (c) describe the frequency scopes of the first and second minigaps, respectively.

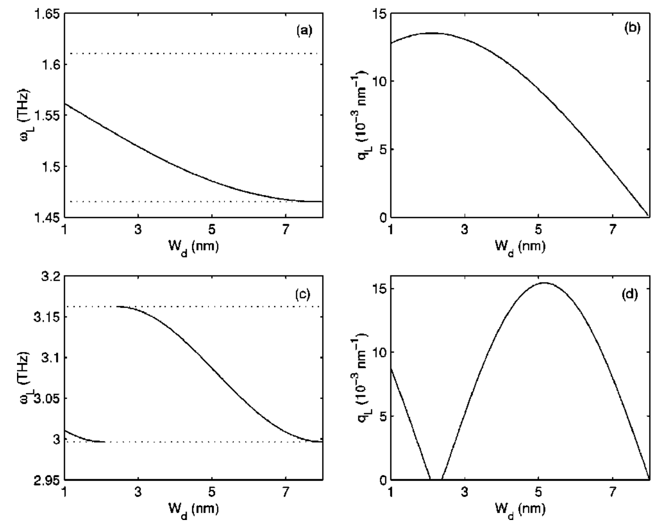

FIG. 3. Dependence of frequency ω and decay factor q of the localized L acoustic modes on the width W_d of the defect layer d in the coupled SL's with a single structure defect layer. Here, $W_a = 3$ nm and $W_b = 8$ nm. Explanations for (a)–(d) are the same as Fig. 2.

decreased with the increase of W_a. These results can be well understood. As is well known, the center frequency of the mth minigap for the folded acoustic phonons is determined by

$$\omega_m = m\tilde{v}\pi/W, \tag{35}$$

where $\tilde{v}$ is the average velocity of the acoustic wave. It is evident that the increase of the period of the SL tends to shift minigaps towards low frequency region. Hence the frequencies of the localized modes are reduced as the width of layer a increases. Similar results can be found as increasing the b-layer width. From Fig. 2(c), we also notice that the minigap gradually narrows and finally vanishes at $W_a \simeq 6.75$ nm. This can be well explained according to approximate formulas of evaluating minigap widths.[15]

q value of the localized modes represents a localization degree of the modes in space. Apparently, we can see that there exists a maximum value in each q-W_a curve in Figs. 2(b) and (d), but the peak positions for different localized modes are different. Compare Fig. 2(b) with Fig. 2(d); we can find the peak value of the second localized mode is higher than that of the first localized mode for the same structural parameters. We also display behaviors of the transverse acoustic phonons in the same coupled SL. Similar features are found.

We now investigate the effect of the width W_d of the defect layer on the localized modes of the longitudinal acoustic phonons. Here, we take $W_a = 3$ nm and $W_b = 8$ nm. Figures 3(a) and (b) show the dependence of the frequency and decay factor of the first localized mode on W_d, and Figs. 3(c) and (d) for the second localized mode. The regions between two horizontal dotted lines represent frequency scope of the first and second minigaps, respectively. It should be noted from Eqs. (7) and (8) that the minigaps are determined by periodic structure of SL and have nothing to do with defect layers. Some main characteristics of the localized states can be described as follows: (i) The frequencies of the localized modes are usually decreased with the increase of the width W_d of the defect layer. Here it is worthy to be pointed out in particular that the localized modes fully vanish at $W_d = 8$ nm $= W_b$. This is because the structure has become a perfect SL when $W_d = 8$ nm. Apparently, there is no localized mode in a perfect SL. The formation of the minibands is attributed to the split of levels due to periodicity coupling between the adjacent quantum wells in the perfect SL. When introducing structural defects into an ideal SL, this periodicity coupling is locally broken down around the structural defect layer. This periodicity-broken coupling leads to the appearance of new splitting levels, different from the splitting levels stemmed from the periodicity coupling. Some of them may lie within the minibands of the SL and develop into the delocalized scattering states, and the other part of them resided in the minigaps of the SL become the localized states. Therefore the localized modes exist only in SL with defect structure. (ii) For some values of W_d, the localized modes also no longer appear. For example, when $2.07 \leqslant W_d \leqslant 2.38$ nm, there is no localized mode in the second minigap. (iii) The closer to the center of the minigap the position of the localized state, the higher is its localization degree.

To further reveal the influence of the width W_d of defect layer on the localized modes, we study the modulus of wave functions of the localization modes. The moduli of the wave functions within the region including four unit cells at each side of the defect layer as well as defect layer itself for the structures in Fig. 3 are illustrated in Fig. 4. The center of the defect layer is chosen as the coordinate center ($Z = 0$). Curves a–c in Fig. 4(a) correspond to $W_d = 2.12$, 5.80, and 7.80 nm in Figs. 3(a) or (b), respectively. Accordingly, their q values are 13.533, 7.172, and 0.681(10^{-3} nm^{-1}). Curves a–d in Fig. 4(b) correspond to $W_d = 1.50$, 3.60, 5.16, and

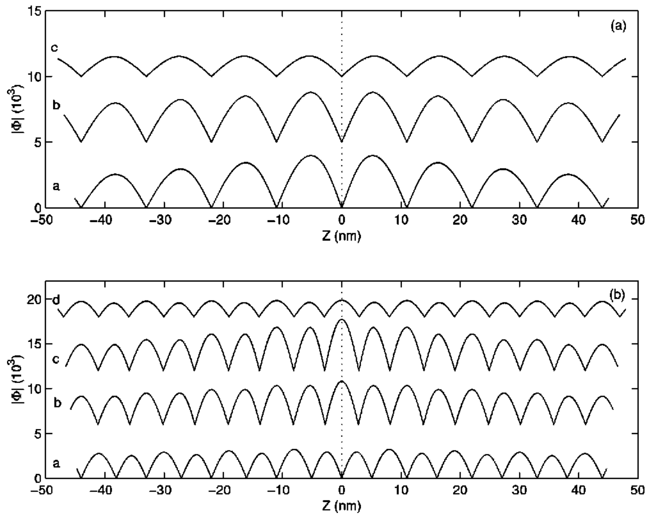

FIG. 4. Moduli of the wave function of the localized L acoustic modes lying in the first and second minigap. Curves a–c in (a) correspond to $W_d=2.12$, 5.80, and 7.80 nm in Figs. 3(a) or (b). Curves a–d in (b) correspond to $W_d=1.50$, 3.60, 5.16, and 7.80 nm in Figs. 3(c) or (d), respectively. Here, we plot the moduli of the wave function within the region including four unit cells at each side of defect layer and defect layer itself in each curve in both (a) and (b). For clarity, two consecutive curves in (a) and (b) are vertically separated by 5×10^3 and 6×10^3, respectively. The center of the defect layer is chosen as the coordinate center $(Z=0)$.

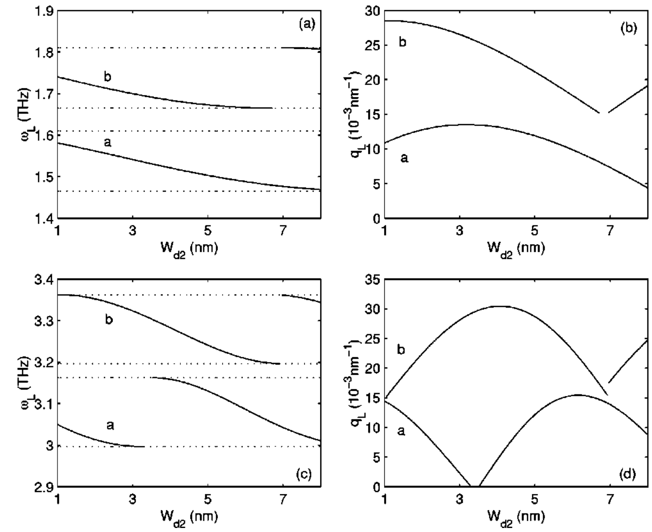

FIG. 5. Dependence of frequency and decay factor of the localized L acoustic modes on W_{d2} in the first and second minigaps in the coupled SL's with the binary defect layer. Here, $W_a=3$ nm, $W_b=8$ nm, and curves a and b correspond to different thicknesses of the defect layer $d1$: $W_{d1}=2$ and 4 nm, respectively. The regions between two dotted lines in (a) and (c) describe the scopes of the frequency of the first and second minigaps, respectively. For clarity, two consecutive curves are separated by 0.2 THz in (a) and (c), and by $15(10^{-3}\ \text{nm}^{-1})$ in (b) and (d), respectively.

7.80 nm in Figs. 3(c) or (d), respectively. Accordingly, their q values are 4.781, 9.758, 15.435, and $1.670(10^{-3}\ \text{nm}^{-1})$, respectively.

From Figs. 4(a) and (b), some characterstics can be addressed as follows: (i) The wave function exhibits a decaying behavior. When the frequency of the localized modes approaches closer to the center of the minigap, the corresponding q value is bigger, and its localization becomes stronger. So q value can serve as a measure of localization degree for the corresponding localized mode. (ii) The number of maxima of the modulus in each cell always coincides with the minigap number. (iii) The wave function of each localized mode has a definite parity due to structural symmetry. The wave function in Fig. 4(a) possesses odd parity. In fact, the wave function of the localized modes lying in the first minigap is of odd parity for $1\ \leqslant W_d \leqslant 8$ nm. However, Fig. 4(b) shows that the parity of the localized mode in case a is odd, while parity of the localized modes in cases b–d is even. As a matter of fact, the parity of the localized modes in the second minigap is odd for $1\leqslant W_d\leqslant 2.07$ nm, while it becomes even as $2.38\leqslant W_d\leqslant 8$ nm. These characteristics are similar to those of the localized electron states in SL's with symmetric defect layers. In our previous work,[30] we made a detailed study on the parity of the localized electron states.

We also consider the cases of the structural defect composed of a material (GaAs). Similar phenomena are observed, too.

We now turn to investigation of the localized modes in SL's with binary structural defect layers, shown in Fig. 1(b). First, let us focus on influences of the defect layers on the localized modes. We fixed $W_a=3$ nm and $W_b=8$ nm. The variations of the frequency and decay factor with W_{d2} are shown in Figs. 5(a) and (b) for the first minigap, and in Figs. 5(c) and (d) for the second minigap, respectively. Curves a and b correspond to different thicknesses of defect layer d_1: $W_{d1}=2$ and 4 nm, respectively. The region between two dotted lines in Figs. 5(a) and (c) represents the scope of the first and second minigaps, respectively.

From Figs. 5(b) and (d) it is clearly seen that the peak value of the curves a and b for the same minigap almost remains unchanged [about $13.533(10^{-3}\ \text{nm}^{-1})$ for the first localized mode and $15.435(10^{-3}\ \text{nm}^{-1})$ for the second localized mode]. As mentioned above, the maximum value of decay factor q corresponds to the frequency of the center of minigap. As soon as this frequency goes through the center of minigap, which is determined by W_a and W_b, the peak of decay factor q will appear necessarily. Their locations shift towards the lower W_{d2} as increasing the width of the defect layer $d1$. These results manifest that the defect layers do not affect the peak value of q and only cause a shift of peak positions. This shows that the effect of the binary defect layer is plausibly equal to that of a single defect layer with certain attaching thickness.

We now begin to envisage the effect of different W_a values on curves ω_L-W_{d2} and q_L-W_{d2} for a fixed $W_{d1}=3$ nm. Figure 6 displays the variations of ω_L and q_L with W_{d2} for different values of W_a in the first minigap and second minigap. The regions between two dotted lines in Figs. 6(a) and (c) represent the scope of the first and second minigaps, respectively. Curves a and b in Fig. 6 correspond to $W_a=2$ and 4 nm, respectively.

We first consider the circumstances of the localized modes in the first minigap, shown in Figs. 6(a) and (b). The scopes of minigap corresponding to a and b in Fig. 6(a) are about 1.777–1.647 and 1.470–1.322 THz, respectively. Accordingly, the maximum values of q, illustrated in Fig. 6(b),

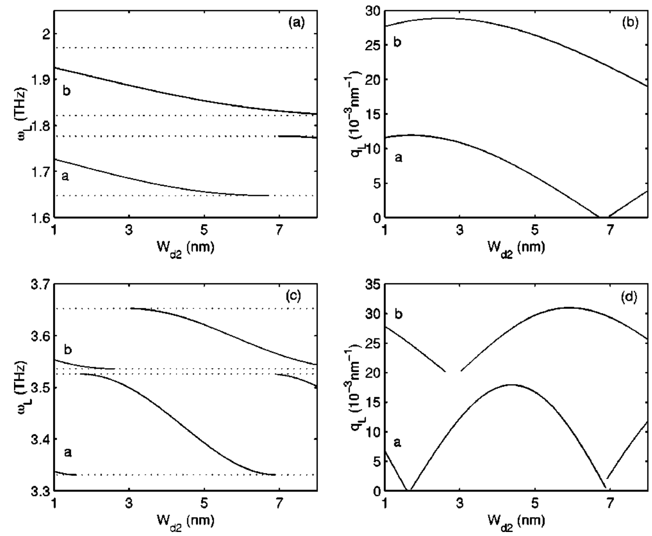

FIG. 6. Dependence of frequency and decay factor of the localized L acoustic modes on W_{d2} in the first and second minigaps in the coupled SL's with the binary defect layer for different values of W_a. Here, $W_{d1}=3$ nm, $W_b=8$ nm, and curves a and b correspond to different thicknesses of the well layer a:$W_a=2$ and 4 nm, respectively. The regions between two dotted lines in (a) and (c) describe the scopes of the frequency of the first and second minigaps. For clarity, two consecutive curves in (a)–(d) have been offset by 0.5 (THz), 15(10^{-3} nm^{-1}), 0.8 (THz), and 20 (10^{-3} nm^{-1}), respectively.

are 11.901 and 13.877 (10^{-3} nm^{-1}), and their positions are located at $W_{d2}=1.70$ and 2.56 nm, respectively. From these calculated results, we reveal the facts that, when W_a is increased, (i) the location of minigap goes down, and its magnitude is increased; (ii) the peak value in curve $q-W_{d2}$ is increased, and its according location shifts right. When exchanging W_a for W_b, the similar results can be obtained in the first minigap. Therefore we can make a conclusion safely that the position and scope of the minigap as well as the peak value in curve $q-W_{d2}$ are dominated by the structural cell of SL.

Now, we investigate situations of the localized modes in the second minigap, shown in Figs. 6(c) and (d). The scopes of minigap, corresponding to a and b in Fig. 6(c), are about 3.526–3.331 and 2.852–2.736 THz. The peak values, corresponding to a and b in Fig. 6(d), are 17.938 and 10.943 (10^{-3} nm^{-1}), and the peak positions are located at $W_{d2}=4.395$ and 5.900 nm, respectively. These calculated results exhibit features apparently different from those in the first minigap: when W_a is increased, (i) the position of minigap is descended, but the scope is narrowed; (ii) the peak value of the curves q_L-W_{d2} is reduced, and its corresponding location shifts right. Moreover, the peak value in the second minigap is evidently higher than that in the first minigap.

According to the results obtained in Fig. 6, we find the fact that for certain structural parameters there is an ideal localization effect in the second minigap, however, the localization degree in the first minigap is low, and vice versa. In other words, we cannot obtain ideal localization effect in the first and second minigaps simultaneously.

IV. SUMMARY

We have studied the property of the localized folded acoustic phonon modes for two types of coupled semi-infinite superlattices with both single and binary structural defect layers. We find that the emergence of the localized folded acoustic phonon modes in the minigaps of the coupled SL's grown along a cubic axis bulk materials is due to the introduction of structural defect layers. The frequency and the localization degree of those localized folded phonon modes strongly depend on the widths of the constituent layers of SL's and the defect layers. In the coupled SL with the single defect layer, the variation of the frequency of the localized modes with the constituent layer width of the SL exhibits a monotonic decrease, however, the profile of the decay factor presents a peak. The variation of the frequency and the localization degree of the localized phonon modes with the width of the defect layer show some interesting characteristics. For example, for some widths of defect layer, there is no localization mode in the minigap; there exist both odd and even parity states in the same minigap. In the study of the localized modes of the coupled SL's with the binary structure defect layers, we find that the effect of the binary structure defect layers on the localization degree is equal to that of a single defect layer with certain attaching thickness. The peak value of the localized modes in curve $q-W_{d2}$ is determined by the width of the constituent layer of the SL. We also find the effect of the structural parameters on the localized modes in the first minigap is quite different from that in the second minigap, and we cannot observe ideal localization effect in the first and second minigaps at the same time. Last, we propose that Raman scattering and phonon transition techniques may be utilized to probe the localized acoustic phonon modes in the structural defect SL's.

ACKNOWLEDGMENT

We gratefully acknowledge the financial support by a research grant from the Chinese National Natural Science Foundation.

*Electronic address: wangxh@aphy.iphy.ac.cn

[1] L. Esaki and R. Tsu, IBM J. Res. Dev. **14**, 61 (1970).

[2] R.E. Camley, B. Djafari Rouhani, L. Dobrzynski, and A.A. Maradudin, Phys. Rev. B **27**, 7318 (1983).

[3] B. Djafari Rouhani, L. Dobrzynski, O. Hardouin Duparc, R.E. Camley, and A.A. Maradudin, Phys. Rev. B **28**, 1711 (1983).

[4] F. Calle, M. Cardona, E. Richter, and D. Strauch, Solid State Commun. **72**, 1153 (1989).

[5] E.H. El Boudouti, B. Djafari-Rouhani, E.M. Khourdifi, and L. Dobrzynski, Phys. Rev. B **48**, 10 987 (1993).

[6] S. Mizuno and S.I. Tamura, Phys. Rev. B **45**, 13 423 (1992); **53**, 4549 (1996).

[7] M. Hammouchi, E.H. El Boudouti, A. Nougaoui, B. Djafari-Rouhani, M.L.H. Lahlaouti, A. Akjouj, and L. Dobrzynski, Phys. Rev. B **59**, 1999 (1999).

[8] R. Peroz-Alvarez, F. Garlia-Moliner, and V.R. Velasco, J. Phys.: Condens. Matter **7**, 2037 (1995).

[9] E.H. El Boudouti, B. Djafari-Rouhani, A. Akjoui, and L. Do-

brzynski, Phys. Rev. B **54**, 14 728 (1996).
[10] C. Colvard, R. Merlin, M.V. Klein, and A.C. Gossard, Phys. Rev. Lett. **45**, 298 (1980).
[11] H. Bragger, G. Abstreiter, H. Jorke, H.J. Herzog, and E. Kasper, Phys. Rev. B **33**, 5928 (1986).
[12] B. Jusserand, D. Paquet, F. Mollot, F. Alexandre, and G. le Roux, Phys. Rev. B **35**, 2808 (1987).
[13] J. Sapriel, J. He, B. Djafari Rouhani, R. Azoulay, and F. Mollot, Phys. Rev. B **37**, 4099 (1988).
[14] D.J. Lockwood, R.L.S. Devine, A. Rodriguez, T. Mendialdua, B. Djafari Rouhani, and L. Dobrzynski, Phys. Rev. B **47**, 13 553 (1993).
[15] P.V. Santos, L. Ley, J. Mebert, and O. Koblinger, Phys. Rev. B **36**, 4858 (1987).
[16] Aishi Yamamoto, Tomobumi Mishina, Yasuaki Masumoto, and Masaaki Nakayama, Phys. Rev. Lett. **73**, 740 (1994).
[17] K. Mizoguchi, K. Matsutani. S. Nakachima, T. Dekorsy, H. Kurz, and M. Nakayama, Phys. Rev. B **55**, 9336 (1997).
[18] Albrecht Bartels, Thomas Dekorsey, Heinrich Kurz, and Klaus Köhler, Appl. Phys. Lett. **72**, 2844 (1998).
[19] T. Mishina. Y. Iwazaki, Y. Masumoto, and M. Nakayama, Solid State Commun. **107**, 281 (1998).
[20] Albrecht Bartels, Thomas Dekorsy, Heinrich Kurz, and Klaus Kohler, Phys. Rev. Lett. **82**, 1044 (1999).
[21] L. Tamm, Phys. Z. Sowjetunion **1**, 733 (1932).
[22] F. Capasso, C. Sirtori, J. Faist, D.L. Sivco, S.N.G. Chu, and A.Y. Cho, Nature (London) **358**, 565 (1992).
[23] M. Zahler, I. Brener, G. Lenz, J. Salzman, E. Cohen, and L. Pfeiffer, Appl. Phys. Lett. **61**, 949 (1992).
[24] M. Zalher, E. Colen, J. Salzman, and E. Linder, Phys. Rev. Lett. **71**, 420 (1993).
[25] C. Sirtori, F. Capasso, J. Faist, and S. Scandolo, Phys. Rev. B **50**, 8663 (1994).
[26] G. Lenz and J. Salzman, Appl. Phys. Lett. **56**, 871 (1990).
[27] G. Ihm, S.K. Noh, and M.L. Falk, J. Appl. Phys. **72**, 5325 (1992).
[28] R.A. Suris and P. Lavallard, Phys. Rev. B **50**, 8875 (1994).
[29] D. Indjin, V. Milanovic, and Z. Ikonic, Phys. Rev. B **52**, 16 762 (1995).
[30] Xue-Hua Wang, Ben-Yuan Gu, Guo-Zhen Yang, and Jian Wang, Phys. Rev. B **58**, 4629 (1998).
[31] Maria Steslicka, Robert Kucharczyk, and M.L. Glasser, Phys. Rev. B **42**, 1458 (1990).
[32] *Semiconductors: Group IV Elements and III–V Compounds*, edited by O. Madelung (Springer, Berlin, 1982).